Journal of Atomic and Molecular Sciences

ISSN 2075-1303

Global Science Press

# Binding Difference of Inhibitors ACD and TDZ to A-FABP Revealed by Molecular Dynamics Simulations

Received: Nov. 4, 2017,
Accepted: Dec. 15, 2017

DOI: 10.4208/jams.110417.121517a

http://www.global-sci.org/jams/

Fangfang Yan[a], Xinguo Liu[a*], Shaolong Zhang[a], Jing Su[a], Qinggang Zhang[a], and Jianzhong Chen[b*]

**Abstract.** Adipocyte fatty-acid binding protein (A-FABP) is abundantly expressed in macrophage and adipocyte, and it is a potential target for the treatment of atherosclerosis and metabolic disease. In this work, binding differences of two inhibitors ACD and TDZ to A-FABP were studied by using principal component (PC) analysis, molecular mechanics generalized Born surface area (MM-GBSA) and solvated interaction energy (SIE) methods. The results show that the binding of inhibitor TDZ to A-FABP is stronger than that of ACD to A-FABP. The calculation of residue-based free energy decomposition and dynamics analysis of hydrogen bonds suggest that hydrophobic interactions and hydrogen bonding interactions play important roles in the structural stability of A-FABP. The information obtained from this work will provide a useful clue for design of effective drugs targeting A-FABP.

## 1. Introduction

Fatty acid binding proteins (FABPs) can reversibly bind to hydrophobic ligands including long chain fatty acids and these kinds of proteins have relatively low molecular weight of (14~15 kDa) [1]. Up to now, at least nine family members of FABPs have been discovered, and adipocyte fatty acid binding protein (A-FABP) is one of the most widely studied members among FABPs [2,3]. A-FABP is the fourth fatty acid binding protein to be discovered, so it is also called fatty acid binding protein 4 (namely FABP4). Structurally, A-FABP consists of two α-helices, ten β-sheets, and the helix-loop-helix domains covering the top of the structures to form a binding pocket for inhibitors (Figure 1.1(A)). This protein, mainly existing in adipose tissue and macrophages [4,5], plays a key role in the regulation of metabolism, inflammation and immune response [6,7]. The bindings of inhibitors to A-FABP can effectively inhibit the development of atherosclerosis, therefore, A-FABP has been a potential target for the treatment of inflammation, atherosclerosis and metabolic disease.

Over the past few years, a series of inhibitors of A-FABP have been reported [8,9] and a number of crystal structures of A-FABP associated with various ligands have been determined [10-12], which provides structural basis for further investigating binding modes of inhibitors to A-FABP. In this study, two inhibitors ACD and TDZ are selected to investigate their binding difference to A-FABP. The structures of ACD and TDZ are shown in Figure 1.1(B-C) [13,14]. The structural difference of two inhibitors results in different binding abilities of ACD and TDZ to A-FABP. Therefore, it is of importance for design of potent inhibitors targeting A-FABP to probe the underlying binding mechanisms of inhibitors ACD and TDZ to A-FABP at atomic levels.

The previous studies demonstrated that molecular dynamics (MD) simulations and binding free energy calculations have been universal tools for investigating structure and dynamics of A-FABP as well as ligands-protein binding mechanisms [15-24]. In current work, the conformational change of A-FABP induced by inhibitor bindings was probed by applying principal component (PC) analysis [25-30]. At the same time, molecular mechanics generalized Born surface area (MM-GBSA) [31-39] and solvated interaction energy (SIE) methods [40,41] were employed to comparatively study binding difference of ACD and TDZ to A-FABP. We expect that this work is able to provide a theoretical guidance for design of effective drugs to treat metabolic disease related with A-FABP.

## 2. Theoretical methods

### 2.1 System preparations

The crystal structures of A-FABP associated with two inhibitors ACD and TDZ were taken from Protein Data Bank (PDB): 3RZY for the *apo* A-FABP [42], 1ADL for the ACD-A-

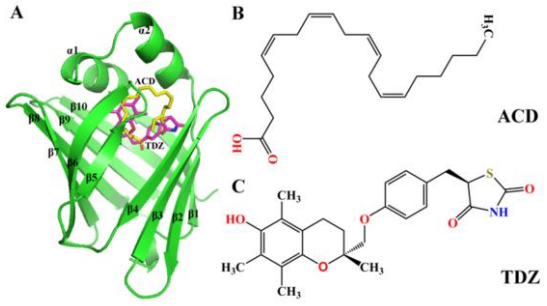


**Figure 1.1**: Structures of molecules: (A) structure of A-FABP in a cartoon diagram and the structures of inhibitors are shown in line modes, (B) inhibitor ACD and (C) inhibitor TDZ.

[a] *School of Physics and Electronics, Shandong Normal University, Jinan, 250014, China*
[b] *School of science, Shandong Jiaotong University, Jinan, 250357, China*
[*] *Corresponding author. E-mail address: liuxinguo@sdnu.edu.cn (X. Liu); chenjianzhong1970@163.com and jzchen@sdjtu.edu.cn (J. Chen).*

FABP system [13] and 2QM9 for the TDZ-A-FABP compound [14]. All the crystal water molecules were remained in the starting structures. All missing hydrogen atoms were added to the corresponding heavy atoms by using the Leap module in Amber 16 [43]. The FF99SB force field was used to describe the protein and water molecules [44]. The general Amber force field (GAFF) was applied to optimize the structures of two inhibitors ACD and TDZ at a semiempirical standard [45,46] and the antechamber module was used to assign AM1-BCC charges to ACD and TDZ [47]. Then, three systems were solved in a truncated octahedral box composing of TIP3P water molecules, keeping a 12.0 Å buffer along each dimension and a certain number of counterions were added to neutralize these systems [48].

### 2.2 MD simulations

Before the starting of MD simulations, it is important to perform energy minimizations on three systems to remove bad contacts between the complex and solvent molecules. The energy optimization of each system was conducted in two steps. Firstly, the harmonic constant of 100 *kcal/mol·Å*$^{-2}$ was used to restrict the complex so as to better optimize the water molecules and counterions. Secondly, all atoms were freely minimized without any restrictions. The steepest descent and conjugate gradient methods were combined to perform energy minimization in each stage. Then, all systems were slowly heated from 0 *K* to 300 *K* in 1 *ns*. After that, the dynamic equilibrium was made on each system at temperature of 300 *K* and constant pressure of 1 *atm*. Finally, 150 *ns* MD simulations were performed on three investigated systems without any restrictions. The Langevin thermostat with a collision frequency of 2.0 *ps*$^{-1}$ was utilized to regulate the temperature of the three systems. All the energy optimization and MD simulations were performed by applying PMEMD module in Amber. The SHAKE algorithm is used to restrain the chemical bonds involving hydrogen atoms, and the time step of dynamic simulation is set to 2 *fs*. The long-range electrostatic interactions were calculated by employing the particle mesh Ewald (PME) method. The electrostatic and van der Waals interactions were truncated at a suitable distance of 9.0 Å.

### 2.3 Principal component analysis

It has been demonstrated that PC analysis is a powerful tool to investigate the conformational change of protein induced by inhibitor bindings [49,50]. In this work, PC analysis was performed on MD trajectories to study the collective motions of A-FABP using the CPPTRAJ module in Amber 16 [51]. The collective motions were described by constructing the positional covariance matrix *C* based on the atomic coordinates, and the elements of the positional covariance matrix *C* can be calculated by the following equation:

$$C_{ij} = < (q_i - < q_i >)(q_j - < q_j >) > \quad (i, j = 1,2,3,3N), \quad (1)$$

where the $q_i$ symbolizes the Cartesian coordinate of $C_\alpha$ atom

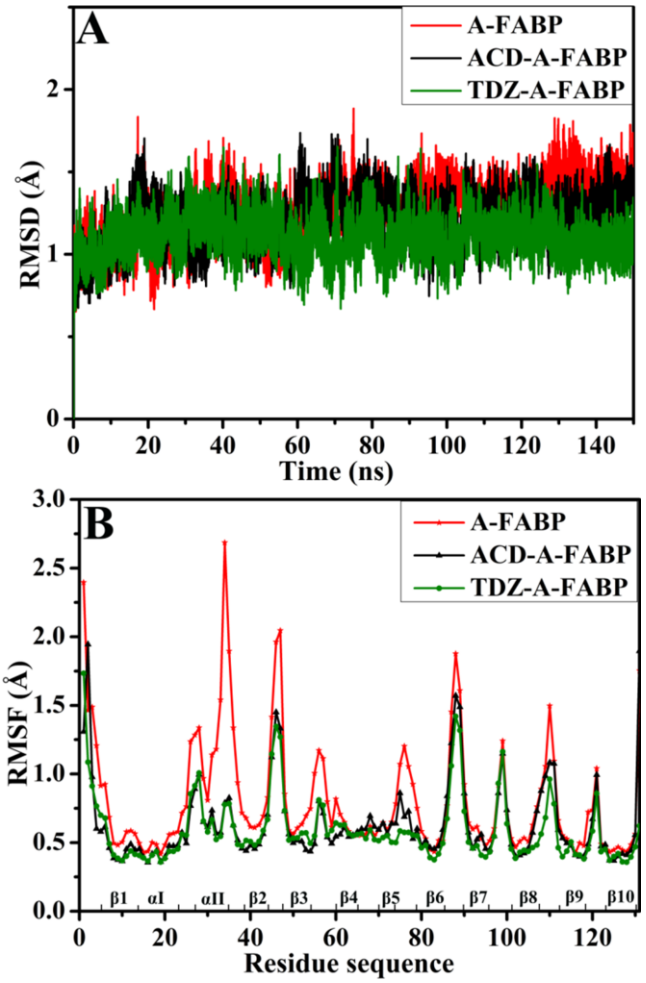


**Figure 3.1.1**: (A) The root-mean-square deviations (RMSDs) of the backbone atoms relative to the corresponding crystal structures as function of simulated time and (B) the root-mean-square fluctuations (RMSFs) of Cα atoms for A-FABP (red), ACD-A-FABP (black) and TDZ-A-FABP (green)

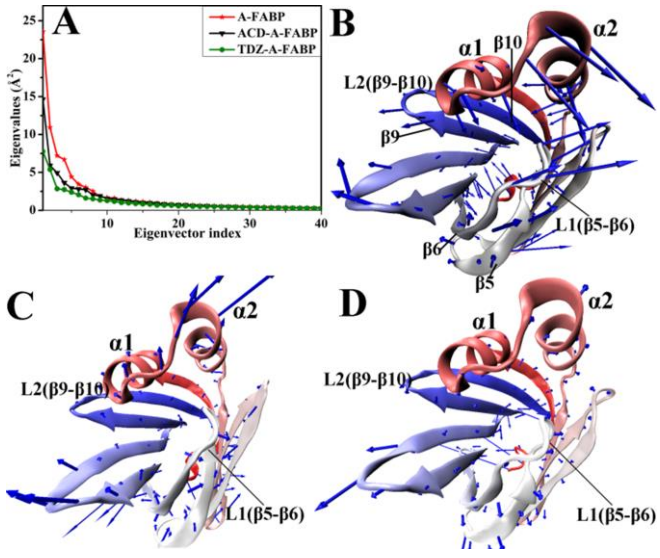


**Figure 3.2.1:** Results of collective motions in A-FABP from principal component analyses. (A) Eigenvalues of the total motions for A-FABP against the corresponding eigenvector indices. Concerted motions of domains along the first eigenvector stemming from principal component analysis: (B) the *apo* A-FABP, (C) the ACD-A-FABP complex and (D) the TDZ-A-FABP complex.

in the *i*th residue and *N* is the number of the $C_\alpha$ atoms involved in construction of the matrix C. All the translations and rotations can be removed by superposing A-FABP on a crystal structure with the least-square fit software. The symmetric matrix *C* can be translated into a diagonal matrix *Λ* of eigenvalues $\lambda_i$ with an orthogonal transformation matrix T:

$$\Lambda = T^T C_{ij} T, \quad (2)$$

in which each column represents the eigenvector that is associated with the direction of motion relative to $< q_j >$, and the corresponding eigenvalue indicates the total mean-square fluctuation of the system along the eigenvector.

### 2.4 MM-GBSA method

MM-GBSA method was employed to compute binding free energies of ACD and TDZ to A-FABP and compare their binding abilities. As for the two systems, 200 conformations were extracted from the last 90 ns of MD trajectories with an interval of 450 *ps* for MM-GBSA calculations. In this method, the binding free energy (*ΔG*) can be calculated by the flowing formula:

$$\Delta G = \Delta E_{ele} + \Delta E_{vdw} + \Delta G_{pol} + \Delta G_{nonpol} - T\Delta S, \quad (3)$$

in which the first two items represent the electrostatic and van der Waals interactions ( $\Delta E_{ele}$, $\Delta E_{vdw}$ ) between inhibitors and protein, respectively. These two items can be obtained from FF99SB force field. The third term indicates the contribution of polar salvation free energy ($\Delta G_{pol}$) to binding affinities, and this term can be acquired by solving the Poisson-Boltzmann equation. In the current calculations, the dielectric constants of solute and solvent were set as 1 and 80, separately. The fourth term is determined by the following empirical relationship:

$$\Delta G_{nonpol} = \gamma \times SASA + \beta, \quad (4)$$

where *SASA* denotes the solvent accessible surface area and the values for empirical parameters γ and β were set to 0.0072 *kcal•mol*$^{-1}$*Å*$^{-2}$ and 0.0 *kcal•mol*$^{-1}$ in this work, respectively. The last term is the contribution of entropy change (-$T\Delta S$ ) to the binding free energy, which can be calculated by Nmode method based on 50 snapshots taken from the above 200 snapshots [52,53].

### 2.5 SIE method

SIE method has been used to successfully predict binding affinities of inhibitors to proteins by using the Sietraj program [41,54]. In order to better calculate binding free energies of these two systems, 200 conformations were taken from the equilibrium trajectories of MD simulations for this computation using the following equation:

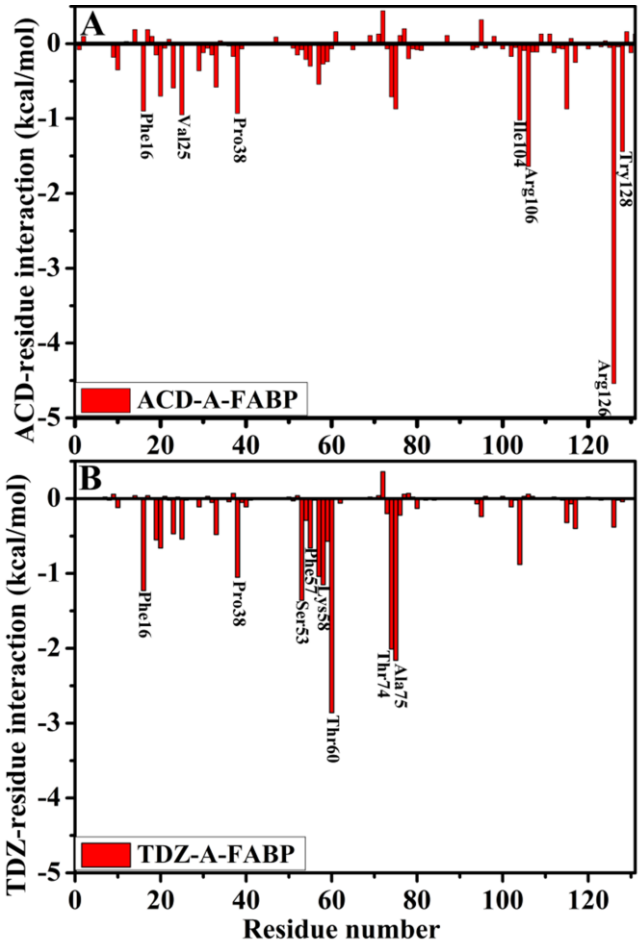


**Figure 3.4.1:** Ligand-residue interactions calculated by applying residue-based free energy decomposition method, only residues stronger than 0.9 kcal/mol in interactions were listed. (A) the ACD-A-FABP complex and (B) the TDZ-A-FABP complex.

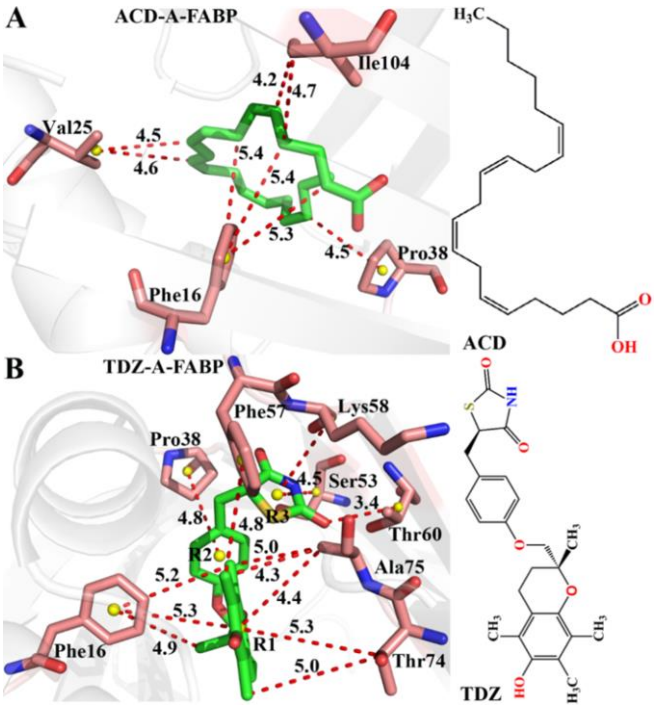


**Figure 3.4.2**: Geometric positions of inhibitors relative to key residues involving significant interactions and the averaged distances between atoms form strong interactions were calculated based on the last 90 ns of MD simulations. (A) the ACD-A-FABP complex and (B) the TDZ-A-FABP complex.

$$\Delta G_{bind}(\rho,\ D_{in},\alpha,\gamma,C) = \alpha \times [\Delta E_c(D_{in}) + \Delta G^R + \Delta E_{vdw} + \Delta G_{cav}(\rho)] + C\ , \quad (5)$$

in which the terms $\Delta E_c$ and $\Delta E_{vdw}$ indicate the contributions of intermolecular Coulomb and van der Waals interactions to binding free energies, respectively. The second term is the reaction energy ($\Delta G^R$), which reflects the changes in the reaction field energy caused by bindings of ACD and TDZ, and it can be obtained by solving the Poisson equation. The last term $\Delta G_{cav}(\rho)$ represents a nonpolar contribution to binding free energies caused by the change of molecular surface area due to inhibitor bindings and is determined by the following equation:

$$\Delta \boldsymbol{E_{cav}} = \boldsymbol{\gamma} \times \boldsymbol{SASA}\ , \quad (6)$$

in which the term *SASA* represents the solvent-accessible surface area. The optimized values of the five parameters α, $D_{in}$, ρ, γ and C are set to 0.1048, 2.25, 1.1, 0.0129 kcal · $mol^{-1}$ ·$Å^{-2}$ and -2.89 kcal/mol, respectively [40,54].

## 3. Results and discussion

### 3.1 The stability and flexibility of inhibitor-A-FABP complexes

To estimate the stabilities of the current three systems during the MD simulations, root mean square deviation (RMSD) of the backbone atoms relative to their crystal structures were calculated and the results were depicted in Figure 3.1.1(A). As shown in Figure 3.1.1(A), the RMSD values of all systems tend to reach equilibrium after 60 *ns* MD simulations. The averaged RMSD of the backbone atoms are 1.27, 1.21 and 1.01 Å for the unbounded A-FABP, ACD-A-FABP and TDZ-A-FABP complexes, separately. These results show that the TDZ-A-FABP compound is more stable than the other two systems in the simulations. The RMSD values indicate that three systems are relatively reliable in the last 90 *ns* of MD simulations for subsequent analyses.

In order to further understand the fluctuations of certain residues relative to its average positions, root mean square fluctuations (RMSFs) of $C_\alpha$ atoms were computed based on the last 90 *ns* MD simulations, and the corresponding results were illustrated in Figure 2B. It is observed from Figure 2B that the residue fluctuations of A-FABP in two complexes have similar tendency to the *apo* A-FABP. The association of two inhibitors with A-FABP generates an obvious decrease in the RMSF values, especially for the residues 35-38, 43-50, 53-60, 73-80. It is found that these residues are mainly distributed near the loops, which indicates that the loops may undergo large conformational changes due to the entrance of inhibitor into the binding pocket of A-FABP. The results suggest that the bindings of inhibitors to A-FABP produces significant contributions to the structural stability of A-FABP, and the presence of inhibitors in binding site may limit the movement of some certain residues.

### 3.2 Principal component analysis

To obtain more information about the conformational changes of A-FABP caused by inhibitor bindings, we carried out PC analyses on the equilibrated MD trajectories. A plot of eigenvalues from the diagonalization of the covariance matrix VS the corresponding eigenvector indices were depicted in Figure 3.2.1(A). One can be observed that the amplitudes of the concerted motions represented by the first few eigenvalues decrease quickly to achieve a series of local fluctuations. The first few eigenvalues of ACD- and TDZ-A-FABP complexes are lower than the ones of the *apo* A-FABP. In fact, the first five components account for 61.9%, 51.6%, and 47.3% of the total motions for the unbounded A-FABP, ACD-A-FABP and TDZ-A-FABP systems, respectively. These results show that bindings of inhibitors exert significant influence on internal dynamics of A-FABP and are favorable for the stabilization of A-FABP structure.

To better investigate the movement of each residues in A-FABP, three porcupine plot were generated by PC analysis and VMD software[55,56](Figure 3.2.1(B)-(D)). In this figure, the direction of the arrow represents the direction of the movement and the length of the arrow suggests the strength of the motion. As shown in Figure 3.2.1(B)-(D), an interesting phenomenon is observed that inhibitor bindings induce significant differences in the movement modes between the bounded A-FABP and the *apo* A-FABP, especially for α1, α2, L1 linking β5-β6 and L2 between β9 and β10. For the *apo* A-FABP (Figure 3.2.1(B)), the two helices α1 and α2 generate strong downward movement, and these motions tend to make the binding cleft become narrow. The loops L1 and L2 also show obvious flexibility. In the case of the ACD- and TDZ-A-FABP complexes (Figure 3.2.1(C)-(D)), both α1 and α2 are in an open state, and the movement directions of two α-helices change about 90˚compared to the *apo* A-FABP. The movement modes of two α-helices in the bounded A-FABP tend to make the binding pocket bigger to accommodate different structural inhibitors ACD and TDZ. Meanwhile, the motional strength of L1 (β5-β6) and L2 (β9-β10) in the bounded state is significantly decreased. Thus, it can be inferred that residues near these regions L1 (β5-β6) and L2 (β9-β10) may have strong interactions with inhibitor so as to limit the motions of these two loops.

### 3.3 Calculations of binding free energies

To acquire more detailed information involving binding affinities of ACD and TDZ to A-FABP, MM-GBSA and SIE methods were applied to calculate binding free energies of two investigated systems, and the results were listed in Table 3-1 (MM-GBSA) and Table 3-2 (SIE).

As shown in Table 3-1, binding free energies are divided into five individual components ($\Delta E_{ele}$, $\Delta E_{vdw}$, $\Delta G_{pol}$, $\Delta G_{nonpol}$ and $-T\Delta S$). The electrostatic interactions ($\Delta E_{ele}$) of ACD and TDZ with A-FABP are -156.50±7.50 and -22.58±4.01 kcal/mol, respectively. The differences in $\Delta E_{ele}$ between ACD-A-FABP and TDZ-A-FABP is 133.92 kcal/mol, and this difference is mainly attributed to hydrogen bonding interactions and charge-charge interactions of carboxyl in ACD with positively charged residues in A-FABP. However, these favorable interactions $\Delta E_{ele}$ are usually opposed by the polar interactions $\Delta G_{pol}$ to form unfavorable interactions ($\Delta G_{ele+pol}$). The van der Waals interactions ( $\Delta E_{vdw}$ ) are

-38.44±3.43, and -49.89±2.50 kcal/mol for ACD- and TDZ-A-PTP1B complexes, respectively, which favors the association of ACD and TDZ with A-FABP, especially for the inhibitor TDZ. Moreover, the non-polar solvation energy ($\Delta G_{nopol}$) provides weak contribution to inhibitor bindings. The binding free energies of ACD and TDZ to A-FABP are -8.14 and -15.62 kcal/mol, separately, and the ranks of our calculated results are consistent with the experimentally determined ones.

For Table 3-2, binding free energies are mainly contributed by intermolecular Coulomb interactions ($\Delta E_c$), van der Waals interactions ($\Delta E_{vdw}$), non-polar interactions ($\Delta G_{cav}$) and reaction energy ($\Delta G^R$). Compared with the ACD-A-FABP complex, $\Delta E_c$ has a weak contribution to the binding of TDZ to A-FABP, while $\Delta E_{vdw}$ generates great contribution to the TDZ binding, which is in agreement with the information in Table 3-1 and the order of the experimental values.

**Table 3.1**: Binding free energies of inhibitors to A-FABP calculated by MM-GBSA method[a]

| Energy | ACD-A-FABP | Std | TDZ-A-FABP | Std |
|---|---|---|---|---|
| $\Delta E_{ele}$ | -156.50 | 7.50 | -22.58 | 4.01 |
| $\Delta E_{vdW}$ | -38.44 | 3.43 | -49.89 | 2.50 |
| $\Delta G_{pol}$ | 161.91 | 6.86 | 38.19 | 2.64 |
| $\Delta G_{nopol}$ | -6.37 | 0.16 | -7.16 | 0.13 |
| $\Delta G^b_{ele+pol}$ | 5.41 | 2.90 | 15.62 | 2.48 |
| $-T\Delta S$ | 26.46 | 4.00 | 25.81 | 2.85 |
| $\Delta G^c_{bind}$ | -12.93 | | -15.62 | |
| $\Delta G^d_{\exp}$ | -7.36 | | -10.67 | |

[a]All values are in kcal/mol. [b] $\Delta G_{ele+pol} = \Delta E_{ele} + \Delta G_{pol.}$

[c]$\Delta G_{bind} = \Delta E_{ele} + \Delta E_{vdw} + \Delta G_{pol} + \Delta G_{nonpol.}$

[d]The experimental values were derived from the experimental Kd values using the equation $\Delta G_{exp} = TRlnK_{\mathrm{d}}$.

**Table 3-2**: Binding free energy of three complexes calculated by SIE method [a]

| Component | ACD-A-PTP1B | Std | TDZ-A-PTP1B | Std |
|---|---|---|---|---|
| $\Delta E_{vdw}$ | -38.64 | 0.48 | -51.36 | 0.61 |
| $\Delta E_c$ | -69.04 | 0.71 | -9.01 | 0.28 |
| $\Delta G_{cav}$ | -9.29 | 0.04 | -10.29 | 0.16 |
| $\Delta G^R$ | 58.27 | 0.49 | 18.73 | 0.58 |
| $\Delta G_{bind}$ | -8.14 | 0.06 | -9.23 | 0.07 |
| $\Delta G^b_{\exp}$ | -7.36 | | -10.67 | |

[a]All values are in kcal/mol. [b]The experimental values were derived from the experimental Kd values using the equation $\Delta G_{exp} = TRlnK_{\mathrm{d}}$.

**Table 3-3**: Main hydrogen bonding interactions formed between inhibitors and A-FABP

| Compound | a Hydrogen bonds | Distance (Å) | Angle(°) | Occupancy (%) |
|---|---|---|---|---|
| ACD-A-FABP | Arg106-NH2-HH21···ACD-O1 | 2.91 | 157.60 | 59.59 |
| | Arg126-NE-HE···ACD-O2 | 2.85 | 153.86 | 69.35 |
| | Arg126-NH2-HH21···ACD-O2 | 2.88 | 147.56 | 61.59 |
| | Arg126-NE-HE···ACD-O1 | 2.85 | 153.89 | 50.70 |
| | Arg126-NH2-HH21···ACD-O1 | 2.88 | 147.79 | 27.55 |
| | Tyr128-OH-HH···ACD-O2 | 2.80 | 156.64 | 87.81 |
| | Tyr128-OH-HH···ACD-C1 | 3.31 | 153.41 | 80.72 |
| | Tyr128-OH-HH···ACD-O1 | 2.97 | 145.45 | 72.65 |
| TDZ-A-FABP | TDZ-NAP-H27···Thr60-OG1 | 2.97 | 158.78 | 80.74 |
| | Thr74-CA-HA···TDZ-OAG | 2.92 | 128.09 | 54.91 |
| | Ala75-N-H···TDZ-OAG | 2.97 | 153.95 | 67.01 |

[a]Hydrogenbonds are determined by the acceptor···donor distance of <3.5Å and acceptor···H-donor angle of >120°.

[b]Occupancy(%) is defined as the percentage of simulation time that a specific hydrogen bond exists.

The above results from calculations of two methods indicate that TDZ can produce stronger association with A-FABP than ACD.

### 3.4 Decomposition of binding affinity into contributions of individual residues

In order to gain the detailed insight into the underlying binding mechanisms of inhibitors to A-FABP, residue-based free energy decomposition method was applied to probe the contribution of individual residues to inhibitor bindings and the corresponding information was depicted in Figure 3.4.1 CPPTRAJ module in Amber 16 was also used to analyze hydrogen bonds between inhibitors and A- FABP, and the corresponding results are given in Table 3-3 and Figure 3.4.3.

For the ACD-A-FABP complex, the interactions of seven residues with ACD are lower than -0.9 kcal/mol, these residues include Phe16, Val25, Pro38, Ile104, Arg106, Arg126 and Tyr128 (Figure 3.4.1(A)) The interaction energies of residues Phe16, Val25, Pro38 and Ile104 with ACD are -0.9, -0.95, -0.93, and -1.02 kcal/mol, respectively, and these interactions mainly come from the hydrophobic interactions of residues with ACD (Figure 3.4.2(A)). It is worth mentioning that the interactions of residues Arg106, Arg126 and Tyr128 mainly stem from electrostatic interactions with ACD. Especially, positively charged residue Arg126 can not only generate strong charge-charge interaction with the carboxyl of ACD, but also forms four hydrogen bonding interactions with inhibitor ACD (Table 3-3 and Figure 3.4.3(A)), which provides strong polar interactions of -4.54 kcal/mol for the ACD binding to A-FABP. The residues Arg106 and Tyr128 also form hydrogen bonding interactions with inhibitor ACD (Table 3-3 and Figure 3.4.3(A)).

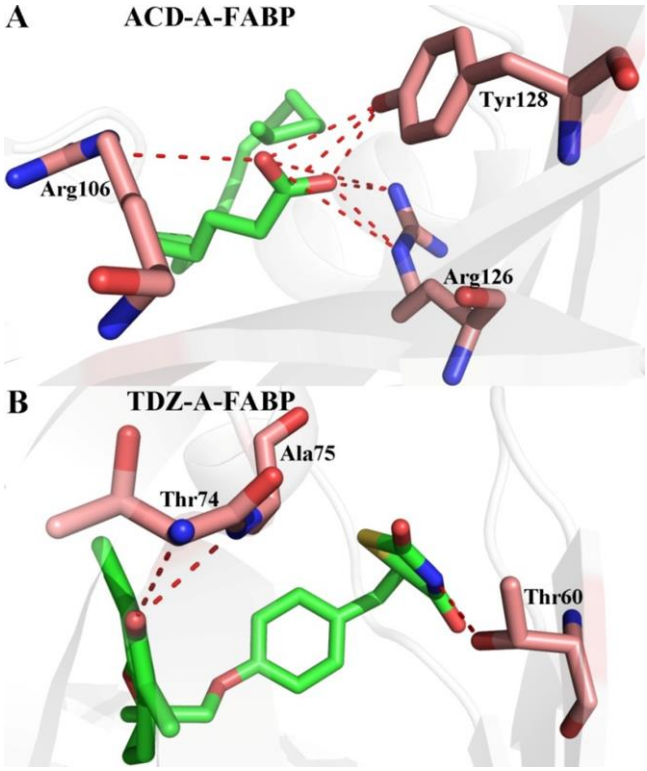


**Figure 3.4.3**: Hydrogen bonding interactions formed between two inhibitors and separate residues in A-FABP: (A) the ACD-A-FABP complex and (B) the TDZ-A-FABP complex.

For the TDZ-A-FABP complex, there are eight residues (Phe16, Pro38, Ser53, Phe57, Lys58, Thr60, Thr74, and Ala75) involving in the main interactions with TDZ (Figure 3.4.1(B)). The contribution of the residue Phe16 is primarily from the π-π and CH-π interactions with the ring R1 and the carbon atoms in the alkyl of TDZ. The residue Pro38 is close to the hydrophobic ring R2, and easy to form the CH-π interaction with the ring R2. The residue Phe57 also generates the CH-π interaction with the carbon atoms in the alkyl of TDZ. The residues Ser53 and Lys58 mainly provide van der Waals interactions for the binding of TDZ to A-FABP, and their interaction strength are –1.36 and -1.58 kcal/mol, respectively. It is worth noting that the energy contributions of three residues Thr60, Thr74, and Ala75 are stronger than -2.0 kcal/mol (-2.86, -2.01, and -2.16kcal/mol, respectively). Except for the van der Waals interactions between the residue Thr60 and the ring R3, there is one hydrogen bond with occupancy of 80.74% between Thr60 and the N atom in the ring R3 of TDZ. The energy contributions of the residues Thr74 and Ala75 not only come from the hydrophobic interactions between these residues and the carbon atoms in the ring R1 of TDZ (Figure 3.4.2(B)), but also stem from the hydrogen bonding interactions between these two residues and the oxygen atom OAG in the inhibitor TDA (Table 3-3 and Figure 3.4.3).

The above analyses show that the hydrogen bonding interactions and Van der Waals interactions are two main driving forces for the binding of inhibitors to A-FABP, and these two kinds of interactions can make the bindings ofinhibitors to A-FABP more stable. The information obtained from this study can provide useful helps for design of effective drugs to treat inflammation and metabolic disease.

## 4. Conclusion

In the current work, 150-ns MD simulations were performed on the *apo* A-FABP, ACD-A-FABP and TDZ-A-FABP complexes to investigate the binding difference including the conformational change of A-FABP and binding abilities of ACD and TDZ to A-FABP. The PC analysis was applied to probe the conformational changes of A-FABP caused by the ACD and TDZ bindings and the results show that the associations of inhibitors with A-FABP have important impact on the internal dynamics of protein, especially for α1, α2, L1 linking β5 and β6 and L2 between β9 and β10. Moreover, MM-GBSA and SEI methods were applied to calculate binding free energies of two inhibitors to A-FABP and the calculated information suggests that TDZ has stronger binding ability to A-FABP than ACD. The binding free energy was further decomposed into the contributions of individual residues and the results proved that hydrogen bonds and hydrophobic interactions play important roles in the bindings of ACD and TDZ to A-FABP. We expect that this work can provide useful guidance for design of potent inhibitors targeting A-FABP.

## Acknowledgments

This work is supported by the National Natural Science Foundation of China (11274205, 11274206, and 11504206) and major development projects of Shandong Jiaotong University.

## References

[1] H. Cai, G. Yan, X. Zhang, O. Gorbenko, H. Wang and W. Zhu, Bioorg. Med. Chem. Lett., 20 (2010) 3675.
[2] A. Zimmerman and J. Veerkamp, Cell. Mol. Life Sci., 59 (2002) 1096.
[3] A. V. Hertzel and D. A. Bernlohr, Trends Endocrin. Met., 11 (2000) 175.
[4] B. Spiegelman, M. Frank and H. Green, J. Biol. Chem., 258 (1983) 10083.
[5] C. R. Hunt, J. Ro, D. E. Dobson, H. Y. Min and B. M. Spiegelman, Proc. Natl. Acad. Sci. U.S.A., 83 (1986) 3786.
[6] K. T. Uysal, L. Scheja, S. M. Wiesbrock, S. Bonner-Weir and G. k. S. Hotamisligil, Endocrinology, 141 (2000) 3388.
[7] J. Hirosumi, G. Tuncman, L. Chang, C. Z. Görgün, K. T. Uysal, K. Maeda, M. Karin and G. S. Hotamisligil, Nature, 420 (2002) 333.
[8] H. Cai, T. Wang, J. Zhao, P. Sun, G. Yan, H. Ding, Y.-i. Li, H. Wang, W. Zhu and K. Chen, Acta Pharmacol. Sin., 34 (2013) 1397.
[9] H. Cai, Q. Liu, D. Gao, T. Wang, T. Chen, G. Yan, K. Chen, Y. Xu, H. Wang and Y. Li, Eur. J. Med. Chem., 90 (2015) 241.
[10] F. Lehmann, S. Haile, E. Axen, C. Medina, J. Uppenberg, S. Svensson, T. Lundbäck, L. Rondahl and T. Barf, Bioorg. Med. Chem. Lett., 14 (2004) 4445.
[11] R. Ringom, E. Axen, J. Uppenberg, T. Lundbäck, L. Rondahl and T. Barf, Bioorg. Med. Chem. Lett., 14 (2004) 4449.
[12] E. Marr, M. Tardie, M. Carty, P. T. Brown, I. K. Wang, W. Soeller, X. Qiu and G. Karam, Acta Crystallog., 62 (2006) 1058.
[13] J. M. Lalonde, M. A. Levenson, J. J. Roe, D. A. Bernlohr and L. J. Banaszak, J. Biol. Chem., 269 (1994) 25339.
[14] R. E. Gillilan, S. D. Ayers and N. Noy, J. Mol. Biol., 372 (2007) 1246.
[15] T. B. Woolf, Biophys. J., 74 (1998) 681.
[16] T. B. Woolf and M. Tychko, Biophys. J., 74 (1998) 694.
[17] F. Ran, E. Nachliel and M. Gutman, Biophys. J., 90 (2006) 1535.
[18] L. L. Duan, G. Q. Feng and Q. G. Zhang, Sci. Rep., 6 (2016) 31488.
[19] J. Chen, J. Wang and W. Zhu, Phys. Chem. Chem. Phys., 19 (2017) 30239.
[20] G. Hu, A. Ma and J. Wang, J. Chem. Inf. Model., 57 (2017) 918.
[21] J. Su, X. Liu, S. Zhang, F. Yan, Q. Zhang and J. Chen, J. Biomol. Struct. Dyn. (2017) DOI:10.1080/07391102.2017.1317666.
[22] M. Yang, X. Zhang and K. Han, Proteins: Struct. Funct. Genet., 78 (2010) 2222.
[23] L. Duan, X. Liu and J. Z. H. Zhang, J. Am. Chem. Soc., 138 (2016) 5722.
[24] J. Wang, Q. Shao, B. P. Cossins, J. Shi, K. Chen and W. Zhu, J. Biomol. Struct. Dyn., 34 (2016) 163.
[25] T. Ichiye and M. Karplus, Proteins: Struct. Funct. Genet., 11 (1991) 205.
[26] R. M. Levy, A. R. Srinivasan, W. K. Olson and J. A. Mccammon, Biopolymers, 23 (1984) 1099.
[27] J. Chen, J. Wang and W. Zhu, Phys. Chem. Chem. Phys., 19 (2017) 3067.
[28] F. Yan, X. Liu, S. Zhang, J. Su, Q. Zhang and J. Chen, J. Biomol. Struct. Dyn. (2017) DOI:10.1080/07391102.2017.1394221.
[29] J. Su, X. Liu, S. Zhang, F. Yan, Q. Zhang and J. Chen, Chem. Biol. Drug Des. (2017) DOI:10.1111/cbdd.13148.
[30] M.-J. Yang, X.-Q. Pang, X. Zhang and K.-L. Han, J. Struct. Biol., 173 (2011) 57.
[31] H. Gohlke and D. A. Case, J. Comput. Chem., 25 (2004) 238.
[32] I. Massova and P. A. Kollman, Perspectives in Drug Discovery & Design, 18 (2000) 113.
[33] V. Tsui and D. A. Case, Biopolymers, 56 (2000) 275.
[34] P. D. Lyne, M. L. Lamb and J. C. Saeh, J. Med. Chem., 49 (2006) 4805.
[35] J. Wang, P. Morin, W. Wang and P. A. Kollman, J. Am. Chem. Soc., 123 (2001) 5221.
[36] L. Duan, G. Feng, X. Wang, L. Wang and Q. Zhang, Phys. Chem. Chem. Phys., 19 (2017) 10140.
[37] G. Hu, A. Ma, X. Dou, L. Zhao and J. Wang, Int. J. Mol. Sci., 17 (2016) 819.
[38] E. L. Wu, Y. Mei, K. Han and J. Z. H. Zhang, Biophys. J., 92 (2007) 4244.
[39] G. Hu, Z. Cao, S. Xu, W. Wang and J. Wang, Sci. Rep., 5 (2015) 16481.
[40] M. Naïm, S. Bhat, K. N. Rankin, S. Dennis, S. F. Chowdhury, I. Siddiqi, P. Drabik, T. Sulea, C. I. Bayly, A. Jakalian and E. O. Purisima, J. Chem. Inf. Model., 47 (2007) 122.
[41] J. Chen, J. Wang and W. Zhu, Plos One, 9 (2014) e99862.
[42] J. M. González and S. Z. Fisher, Acta Crystallog., 71 (2015) 163.
[43] D. A. Case, R. M. Betz, D. S. Cerutti, III. Cheatham, T. E., T. A. Darden, R. E. Duke, T. J. Giese, H. Gohlke, A. W. Goetz, N. Homeyer, S. Izadi, P. Janowski, K. Kaus, A. Kovalenko, T. S. Lee, S. LeGrand, P. Li, C. Lin, T. Luchko, R. Luo, B. Madej, D. Mermelstein, R. M. Merz, G. Monard, H. Nguyen, H. T. Nguyen, I. Omelyan, A. Onufriev, D. R. Roe, A. Roitberg, C. Sagui, C. L. Simmerling, W. M. Botello-Smith, J. Swails, R. C. Walker, J. Wang, R. M. Wolf, X. Wu, X. L. and P. A. Kollman, (2016).
[44] L. Yang, C. H. Tan, M. J. Hsieh, J. Wang, Y. Duan, P. Cieplak, J. Caldwell, P. A. Kollman and R. Luo, J. Phys. Chem. B, 110 (2006) 13166.
[45] J. Wang, R. M. Wolf, J. W. Caldwell, P. A. Kollman and D. A. Case, J. Comput. Chem., 25 (2004) 1157.
[46] J. Chen, J. Wang and W. Zhu, Sci. Rep., 6 (2016) 36900.
[47] A. Jakalian, D. B. Jack and C. I. Bayly, J. Comput. Chem., 23 (2002) 1623.
[48] W. L. Jorgensen, J. Chandrasekhar, J. D. Madura, R. W. Impey and M. L. Klein, J. Chem. Phys., 79 (1983) 926.
[49] E. Papaleo, P. Mereghetti, P. Fantucci, R. Grandori and L. D. Gioia, J. Mol. Graph. Model., 27 (2009) 889.
[50] C. Nikita, T. E. Wales, R. E. Joseph, S. E. Boyken, J. R. Engen, R. L. Jernigan and A. H. Andreotti, Plos Comput. Biol., 12 (2016) e1004826.
[51] D. R. Roe and T. E. Cheatham III, J. Chem. Theory Comput., 9 (2013) 3084.

[52] B. Xu, H. Shen, X. Zhu and G. Li, J. Comput. Chem., 32 (2011) 3188.
[53] J. Chen, Rsc Adv., 6 (2016)58573.
[54] Q. Cui, T. Sulea, J. D. Schrag, C. Munger, M. N. Hung, M. Naïm, M. Cygler and E. O. Purisima, J. Mol. Biol., 379 (2008) 787.
[55] W. Humphrey, A. Dalke and K. Schulten, J. Mol. Graph., 14 (1996) 33.
[56] J. Chen, Chem. Biol. Drug Des., 89 (2017) 548.